Human heart

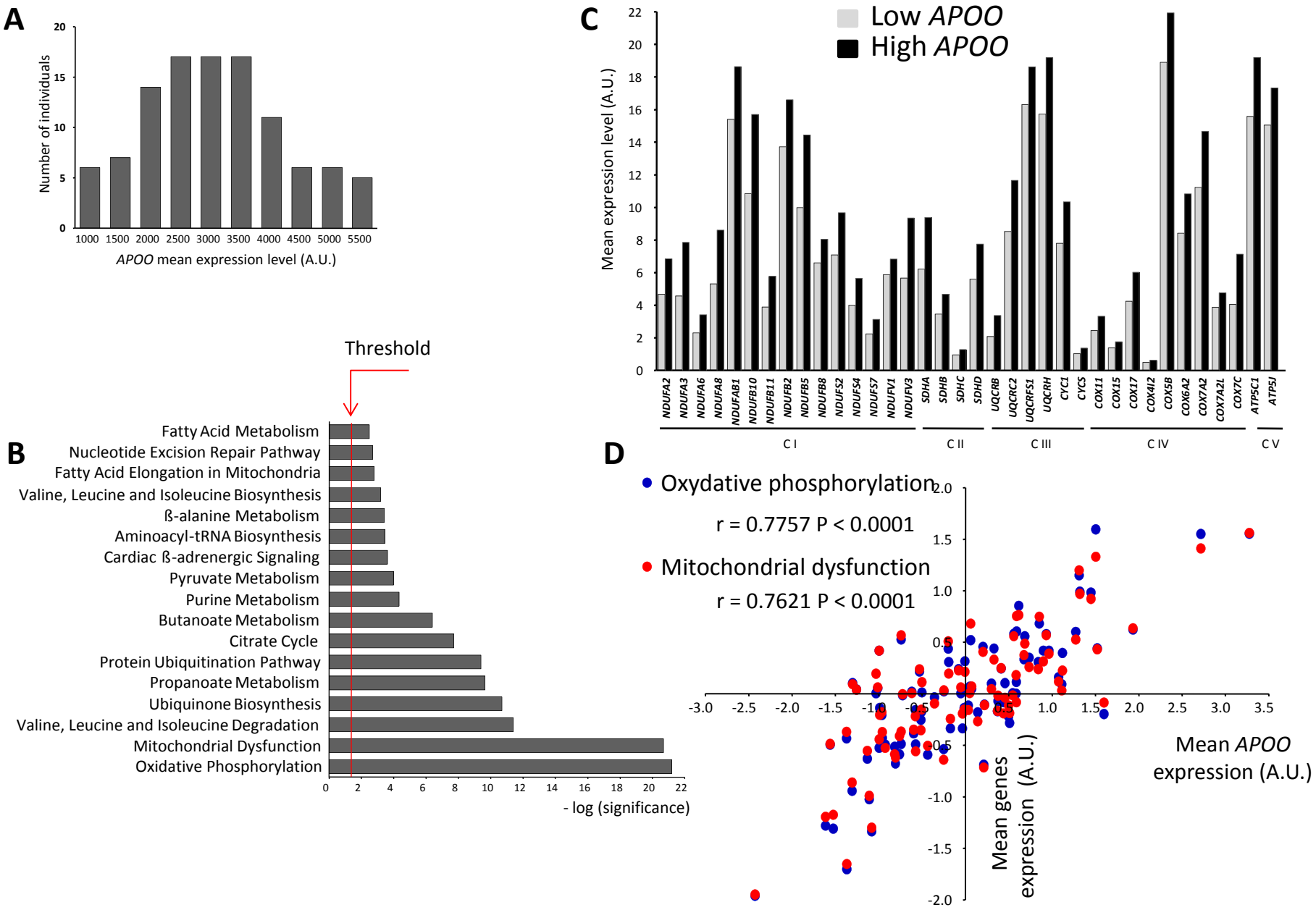
A
Number of individuals
APOO mean expression level (A.U.)
B
Threshold
Fatty Acid Metabolism
Nucleotide Excision Repair Pathway
Fatty Acid Elongation in Mitochondria
Valine, Leucine and Isoleucine Biosynthesis
ß-alanine Metabolism
Aminoacyl-tRNA Biosynthesis
Cardiac ß-adrenergic Signaling
Pyruvate Metabolism
Purine Metabolism
Butanoate Metabolism
Citrate Cycle
Protein Ubiquitination Pathway
Propanoate Metabolism
Ubiquinone Biosynthesis
Valine, Leucine and Isoleucine Degradation
Mitochondrial Dysfunction
Oxidative Phosphorylation
- log (significance)
C
Low APOO
High APOO
Mean expression level (A.U.)
NDUFA2 NDUFA3 NDUFA6 NDUFA8 NDUFAB1 NDUFB10 NDUFB11 NDUFB2 NDUFB5 NDUFB8 NDUFS2 NDUFS4 NDUFS7 NDUFV1 NDUFV3
SDHA SDHB SDHC SDHD
UQCRB UQCRC2 UQCRFS1 UQCRH CYC1 CYCS
COX11 COX15 COX17 COX4I2 COX5B COX6A2 COX7A2 COX7A2L COX7C
ATP5C1 ATP5J
C I C II C III C IV C V
D
Oxydative phosphorylation
r = 0.7757 P < 0.0001
Mitochondrial dysfunction
r = 0.7621 P < 0.0001
Mean genes expression (A.U.)
Mean APOO expression (A.U.)

Supplemental figure 1

GEO database data mining associates *APOO* expression with mitochondrial dysfunction in human heart. (**A**) Distribution of *APOO* mRNA levels extracted from 1O7 independent human heart Affymetrix microarrays, obtained from the GEO repository. (**B**) Ingenuity Pathway Analysis performed using a log ratio of differential gene expression calculated using human heart microarray data from patients undergoing cardiac transplantation and from "normal" organ donors with the highest and the lowest *APOO* expression level respectively. Threshold designates p-value cutoff for pathways significantly enriched in differentially expressed genes (Ingenuity default). (**C**) *APOO* is associated with a rise in the expression of oxidative phosphorylation genes in human heart. Comparison of gene expression levels for members of the oxidative phosphorylation pathway between human heart microarrays with the highest (High *APOO*) and the lowest (Low *APOO*) *APOO* expression level, organized by mitochondrial complex CI to CV. (**D**) Correlation between the expression level of human heart *APOO* and mitochondrial genes selected by functional pathway. Gene expression data were obtained from the GEO database. Expression levels (log10) are indicated as arbitrary units (A.U.).

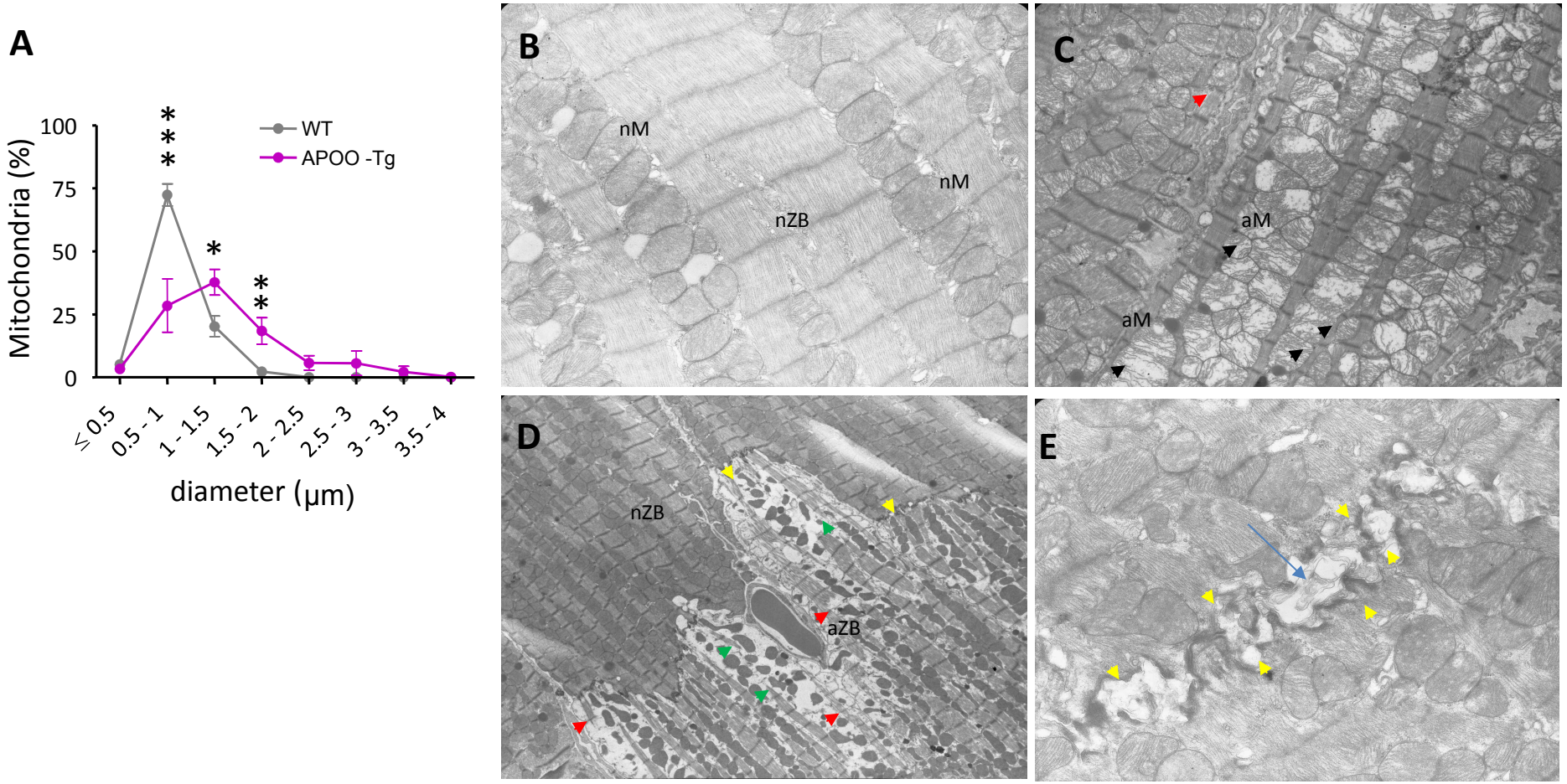

Supplemental figure 2

Transmission electron microscopy analysis of mouse heart shows that a 3-fold APOO overexpression is associated with irreversible degeneration in the myocardium. (**A**) Mitochondrial diameter was measured on transmission electron microscopy of WT (n = 5) and APOO-Tg (n = 5) myocardial sections. 281 and 279 mitochondria were respectively analyzed for WT and APOO-Tg mice. (**B**) WT longitudinal myocardial sections (x15,000). (**C**), (**D**) and (**E**) APOO-Tg longitudinal myocardial sections (x12,000, x3,000 and x15,000 respectively). Normal mitochondrion (nM), Normal Z bands (nZB), Black arrows point to markedly dilated, irregular and altered mitochondria (aM). Green arrows show myofibrillar disarray. Red arrows point to abnormal Z bands (aZB). Blue arrow shows multilamellar bodies. Yellow arrows show widened intercellular junctions *p < 0.05, **p < 0.01, ***p < 0.001. Data represent mean ± SEM.

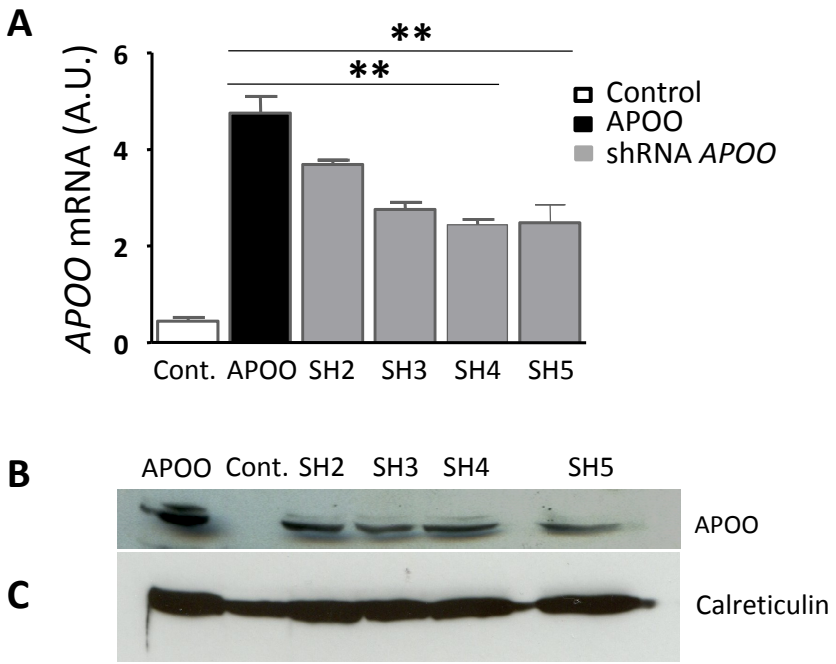

Supplemental figure 3

APOO expression in transfected H9c2 cardiac myoblasts. (A) *APOO* mRNA levels in control cardiac myoblasts and transfectants overexpressing APOO (APOO, 55 kDa). SH2, SH3, SH4 and SH5 indicate 4 independent APOO clones subsequently transfected with 4 different shRNA *APOO* expression vectors (B) APOO Western blot analysis with total protein extracts prepared from control, APOO and shRNA*APOO* cells. (C) Equal lane loading and transfer were verified by probing the same membrane with calreticulin (48 kDa) antibody. Representative data from one experiment is shown. Experiments were repeated three times. **$p < 0.01$. Data represent mean ± SEM.

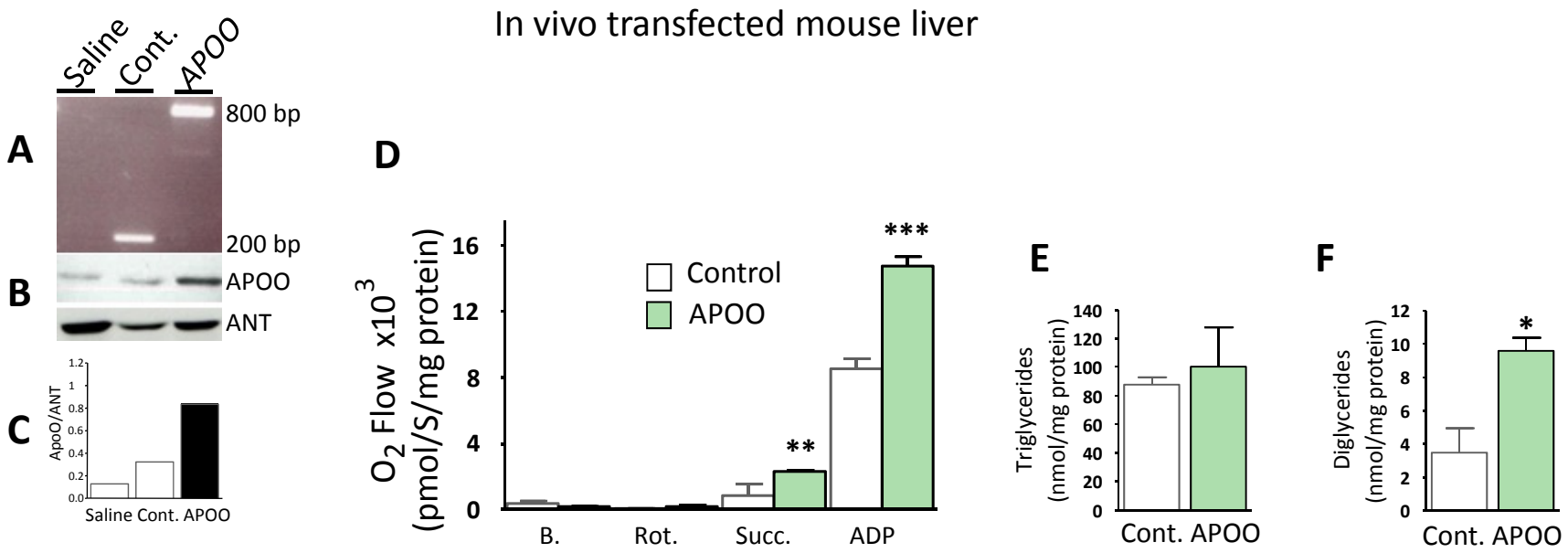

Supplemental figure 4

APOO expression and function in transfected mouse liver. (**A**) 2 % ethidium bromide stained agarose gel electrophoresis of PCR amplified products obtained from mouse liver after hydrodynamics-based in vivo liver transfection by rapid tail vein injection of control (n=12), *APOO* expression vector (n=12), and saline (n=12). (**B**) Western blot of protein extracts from isolated liver mitochondria probed with APOO (55 kDa) antibody shown above the loading/transfer control performed by probing the transferred membrane with ANT (33 kDa) antibody. (**C**) *ImageJ* quantification of the APOO to ANT signal. (**D**) Oxygen consumption of mitochondria isolated from the liver 24 h after hydrodynamics-based in vivo transfection of control (n=12) and APOO (n=12) expression vectors with the following treatments: basal (B), 2.5 µM rotenone (Rot), 5 mM succinate (Succ), and 300 µM adenosine diphosphate (ADP). (**E**) triglycerides and (**F**) Diglycerides levels in the liver after hydrodynamics-based in vivo liver transfection by a rapid tail vein injection of control (n = 12) and APOO (n = 12) expression vectors. *p < 0.05, **p < 0.01, ***p < 0.001. Data represent mean ± SEM.

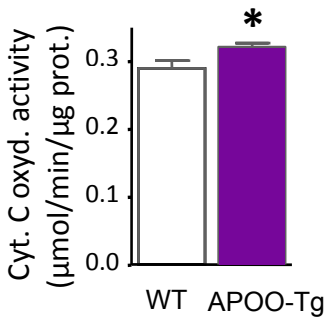

Supplemental figure 5

Cytochrome C oxidase (COX) activity in hearts from wild type (WT, n = 29) and APOO (APOO-Tg, n = 32) mice. *$p < 0.05$. Data represent mean ± SEM.

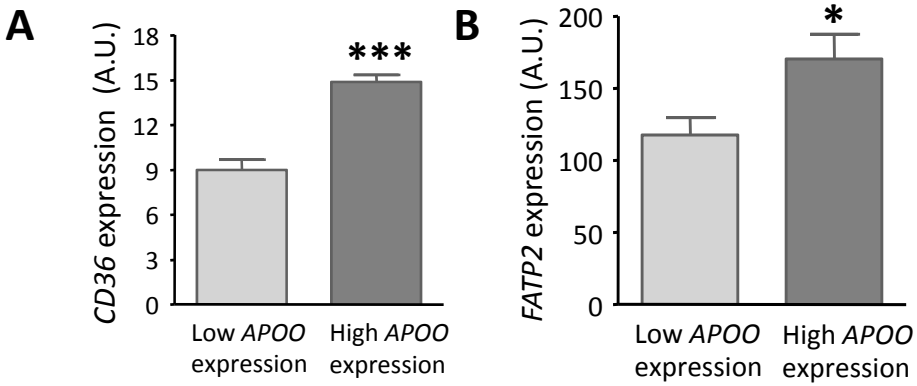

Supplemental figure 6

ApoO is associated with high expression of *CD36* and *FATP2* in human heart. Comparison of (**A**) *CD36* and (**B**) *FATP2* expression levels from human heart microarray data sets (obtained from GEO) from patients with reduced (Low) and elevated (High) *APOO* expression levels. *$p < 0.05$, ***$p < 0.001$. Data represent mean ± SEM.

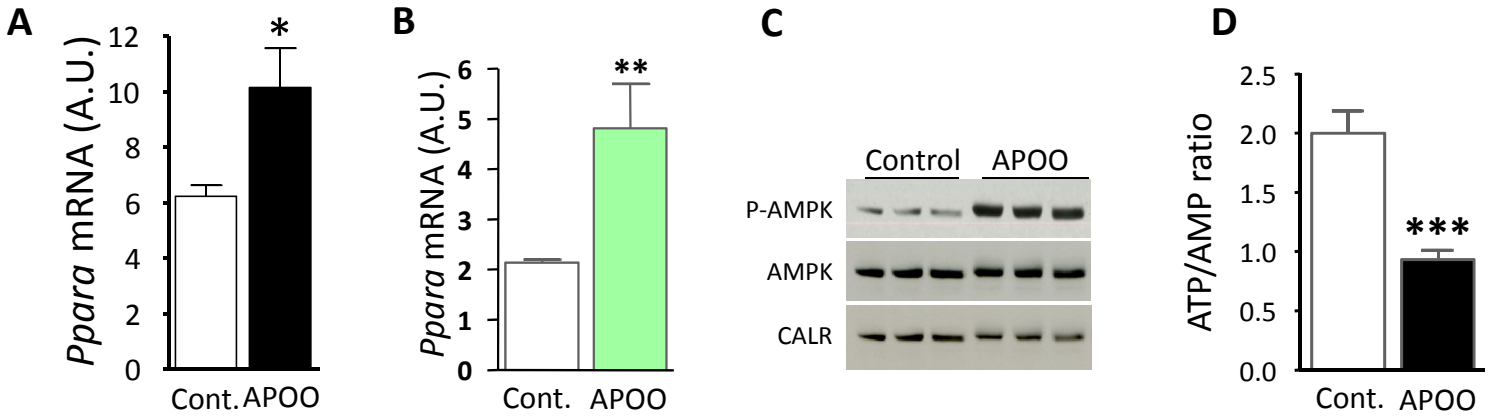

Supplemental figure 7

APOO induces *Ppara* expression, AMPK activation and energy deficiency. (**A**) *Ppara* mRNA level in control and APOO cells (n = 4). (B) *Ppara* mRNA levels in mouse liver after hydrodynamics-based in vivo liver transfection by a rapid tail vein injection of control (n = 12) or APOO (n = 12) expression vectors. (**C**) Phosphorylated AMPK (Thr172) (P-AMPK) and non Phosphorylated AMPK (AMPK) western blot analysis with protein extracts prepared from control and APOO cells. Equal lane loading and transfer were verified by probing the membrane with calreticulin (CALR, 48 kDa) antibody. Representative data from one experiment is shown. Experiments were repeated three times. (D) ATP/AMP ratio in control and APOO cells. *$p < 0.05$, **$p < 0.01$, ***$p < 0.001$. Data represent mean ± SEM.

Supplemental methods

Measurement of the mouse heart mitochondria size. Transmission electron microscopy pictures of heart sections were used for mitochondria diameter measurement. Mitochondria were counted and their size distribution sorted according to the percentage of mitochondria with a given measured diameter. 281 and 279 mitochondria were respectively analyzed for WT and APOO-Tg mice.

RT-qPCR analyses. Total RNAs from tissues samples, including human and mouse hearts or cultured H9c2 cardiomyoblasts were purified using RNeasy kit (Qiagen) in a QIAcube (Qiagen) automated apparatus. Total RNAs integrity was checked by Experion capillary electrophoresis (Bio-Rad). Samples with RNA Quality Indicator ≥ 8.5 / 10 were selected for analyses. Total RNAs were precisely quantified using RiboGreen and a Victor™ X5 2030 multilabel reader (Perkin Elmer).

Oligonucleotides were designed with PerlPrimer (1) software and synthesized by Eurogentec Company. Real-time PCR was performed in a MyiQ™ realtime PCR apparatus (Bio-Rad) using SurePrime kit reagents (MP Biomedicals). The primers used were:

forward 5'-ACATGATCTTCAAGGCGTACCG-3' and reverse 5'-AGTGGACGAACCAGAGAGGTATG-3' for *Nadh dh*,

forward 5'-TGCTACAGCATGTGTGGATGTGAG-3' and reverse 5'-AAAGACCCTGCCTCAACAAGTGG-3' for *Ndufa7*,

forward 5'-AAAGGACGAGAGTGTGGGATGG-3' and reverse 5'-CACTAGGCACACCATCAGGTTTGG-3' for Cytochrome b5,

forward 5'-CTTTTCCAGCCGCTTCCACA-3' and reverse

5’- TGGCTGGCAGGGAATGCA -3’ for human *FATP4*,

forward 5’-TGAGATGGCCTGAGCTATCTG-3’ and reverse 5’-

GCCCGATGTGTAGATGTAGAA-3’ for mouse *Fatp4*,

forward 5’-CTCAGCAGGAAACATTGTGG-3’ and reverse

5’CAGTTGTACTTGATACAGTCATCC3’ for rat *Fatp4*,

forward 5’-TGGCTTATTGAGACTGGGAC-3’ and reverse

5’-AAAGCAACAAACATCACCAC-3’ for human *CD36*,

forward 5’-ATGGGCTGTGATCGGAACTG-3’ and reverse 5’-

GTCTTCCCAATAAGCATGTCTCC-3’ for mouse *Cd36*,

forward 5’-GCTTGAATCCTAACGAAGATGAG-3’ and reverse 5’-

GGCTTGACCAGTATGTTGAC-3’ for rat *Cd36*,

forward 5’-GGGTGGTTGGGTGAGACTC-3’ and reverse

5’-AGACACGTAAGGAAAACGCATTA-3’ for human *BAX*,

forward 5’-AGGATGCGTCCACCAAGAAG-3’ and reverse

5’-TCCTCTGCAGCTCCATATTGC-3’ for mouse *Bax*,

forward 5’-TGCAGACGGCAACTTCAACT-3’ and reverse

5’-TGATCAGCTCGGGCACTTTA-3’ for rat *Bax*,

forward 5’-CCCCTTGGCGTGTCTCTCT-3’ and reverse

5’-TCTCGGCAATTTACACTTGCA-3’ for mouse *Bcl2*,

forward 5’-GCAGTAATCATGTACACAAGTGG-3’ and reverse

5’-GACATCTTGCTGTCCTAGTTCTG-3’ for human *ACSL3*,

forward 5’-TGCGTATGCAAACAGCTACCATTC -3’ and reverse

5’- TTCCATCTCGCTGCTGTTACAC -3’ for mouse *Acsl3*,

forward 5’-GTGCCTTTCTGTCGGGATGT-3’ and reverse

5’-TCTGCTTTCAGTTTTGCTTTCTCA-3’ for human *PPARA*,

forward 5'-ATTCGGCTGAAGCTGGTGTAC-3' and reverse 5'-CTGGCATTTGTTCCGGTTCT-3' for mouse and rat *Ppara*, forward 5'-AACACTTACAAGCCAAACCA-3' and reverse 5'-GCGTTCAATAGTCTTGTTCTC-3' for human *PGC-1A*, forward 5'-GCCCGAGCAATCTGAGTTGTAC-3' and reverse 5'-GGCCGTTTAGTCTTCCTTTCCT-3' for mouse *Pgc-1a*.

Microscopy. Transmission electron microscopy. The tissues were fixed in 2 % glutaraldehyde in 0.1 M Sorensen phosphate buffer (pH 7.4) for 4 h at 4°C, washed overnight in 0.2 M phosphate buffer and then post-fixed for 1 h at room temperature with 1 % osmium tetroxide in 250 mM saccharose and 0.05 M phosphate buffer. The samples were then dehydrated in a series of graded ethanol solutions, followed by propylene oxide, and embedded in an Epon-araldite resin (Embed 812-Araldite 502, Electron Microscopy Sciences). Finally, the tissues were sliced into 70-nm thick sections (Ultracut Reichert Jung) and mounted on 100-mesh collodion-coated copper grids prior to staining with 3 % uranyl acetate in 50 % ethanol and Reynold's lead citrate. The adhering cells were fixed and washed as above and stained overnight in 2 % uranyl acetate. Examinations were carried out on a transmission Hitachi HU12A electron microscope at an accelerating voltage of 75 kV.

Confocal microscopy. Fluorescent detection of SNAP-tagged APOO in pSNAP-APOO-transfected cardiac myoblasts was performed using SNAP-Cell^{TM} TMR-Star fluorescent substrate according to the manufacturer's protocol (New England Biolabs). Briefly, cells expressing SNAP-tag APOO were incubated for 30 min at 37 °C, 5 % CO_2 with 2 µM dye substrate. The cells were then washed three times with tissue culture medium and incubated in fresh medium for 30 min. The cells were imaged with an excitation at 543 nm and an emission at 580 nm on a Zeiss LSM 510 confocal microscope (Carl Zeiss Meditec).

Fluorescence detection of Bodipy-Palmitate (Life Technologies) was performed in subconfluent cells incubated 2 min with Bodipy-Palmitate 1 µM, washed twice in PBS and fixed in 4 % formaldehyde for 15 min at room temperature followed by 5 min at -20 °C. Cells were then washed 3 times in PBS and covered with fluorescent mounting medium and coverslips before being analyzed on a Zeiss LSM 510 confocal microscope (Carl Zeiss Meditec).

Enzyme activity. Palmitate preparation and Caspase-3 activity monitoring. Palmitate preparation and Caspase-3 activity measurements were performed as previously described (2). Caspase-3 assays were performed using the Caspase-3 Substrate IV Fluorogenic substrate (VWR) and a Victor™ X5 2030 multilabel reader (Perkin Elmer)

Acyl-CoA synthetase activity. Acyl-CoA synthetase activity was performed as published (3).

Cytochrome C oxydase activity. Cytochrome C oxydase activity was measured as recommended using Cytochrome C oxidase Assay Kit (Sigma Aldrich) and a Victor™ X5 2030 multilabel reader (Perkin Elmer).

Measurement of O_2 consumption. O_2 flows were measured using an OROBOROS Oxygraph-2k (Oroboros Instruments) and standard Oroboros procedures. Calculation of the respiration control index (RC) was done by dividing oxygen consumption in the presence of CCCP by that measured with oligomycin (4, 5). RC indicates the tightness of the coupling between respiration and phosphorylation.

Reactive oxygen (ROS) species assessment. 5-(and-6)-carboxy-2',7'-dichlorofluorescein diacetate (carboxy-DCFDA) was used as recommended by the manufacturer (Life Technologies) with a Victor™ X5 2030 multilabel reader (Perkin Elmer).

ATP and AMP quantification. Intracellular ATP and AMP were quantified using liquid chromatography coupled to Mass Spectrometry (LC-MS/MS) (6). Briefly, APOO and control cells were rinsed twice with ice cold 0.9 % NaCl (w/v) solution and immediately frozen at -

80°C. Cells were scraped on dry ice in 4 ml of methanol/H2O (80/20). Cell suspensions were centifugated 5 min (-10°C, 2000g). The supernatant was kept at -80°C. The pellet was resuspended in 500 µl methanol/H2O (-80°C), kept 15 min on dry ice and centifugated 5 min (-10°C, 2. 000 g). The supernatant was added to the previous one and maintained at -80°C. This procedure was repeated twice. Methanol was evaporated and the samples were kept at -80°C until analysis. For quantitative analysis, an internal standard produced by yeast grown on U-13C glucose was added (7, 8). Finally, samples were run on a Dionex ionic chromatographic system, using an EGC KOH cartridge and an IonPac Analytical AS11 column and analyzed on a Qtrap4000 (Applied Biosystems) set in MRM mode (6).

Lipids profiling. Cells or tissues were homogenized in 2 ml of methanol / 5 mM EGTA (2 : 1 v/v) with FAST-PREP (MP Biochemicals). 50 µl was removed and evaporated, the dry pellets were dissolved in 0.2 ml of NaOH (0.1 M) overnight, and proteins were measured with the Bio-Rad assay.

Neutral lipid molecular species analysis. Lipids were extracted in chloroform/methanol/water (2.5: 2.5: 2.1 v/v/v) (9), in the presence of internal standards: 3 µg stigmasterol, 2 µg 1,3-dimyristine, 3 µg cholesteryl heptadecanoate, and 5 µg glyceryl triheptadecanoate. Chloroform phases were evaporated. Neutral lipids were separated over SPE columns (Macherey Nagel glass Chromabond pure silica, 200 mg). The extract was applied on the cartridge in 20 µl of chloroform and neutral lipids were eluted with 2 ml of chloroform: methanol solution (90: 10 v/v). The organic phase was evaporated and dissolved in 20 µl of ethyl acetate. 1 µl of the lipid extract was analyzed by gas-liquid chromatography on a FOCUS Thermo Electron system using Zebron-1 Phenomenex fused silica capillary columns. Oven temperature was programmed from 200 °C to 350 °C at a rate of 5 °C per min using hydrogen (0.5 bar) as the carrier gas. The injector and the detector were at 315 °C and 345 °C, respectively.

Fatty Acid Methyl Ester (FAME) quantification. Homogenates were dried in the presence of 2 µg of the internal standard, glyceryl triheptadecanoate, and transmethylated in 1 ml 14 % boron trifluoride methanol solution (Sigma Aldrich) and 1 ml hexane at 55 °C for 1 h. After addition of 1 ml water to the extract, FAMEs were extracted with 3 ml hexane, evaporated and dissolved in 20 µl ethyl acetate. FAMEs (1 µl) were analyzed by gas-liquid chromatography (10) on a Clarus 600 Perkin Elmer system using Famewax RESTEK fused silica capillary columns. Oven temperature was programmed from 110 °C to 220 °C at a rate of 2 °C per min and the carrier gas was hydrogen (0.5 bar). The injector and the detector were at 225 °C and 245 °C, respectively.

Western blots. Membrane preparations were performed as described (11).

Cardiac or liver tissue was disrupted with mammalian MCL-1 cell lysis kit solution (Sigma Aldrich) in presence of protease inhibitors. Procedures were performed according to the manufacturer's protocol. Western blot procedures were performed as described previously (12). Actin, ANT, AMPK-P, AMPK, Calreticulin antibodies were from Clinisciences.

1. Marshall, O.J. 2004. PerlPrimer: cross-platform, graphical primer design for standard, bisulphite and real-time PCR. *Bioinformatics* 20:2471-2472.
2. Hickson-Bick, D.L., Buja, L.M., and McMillin, J.B. 2000. Palmitate-mediated alterations in the fatty acid metabolism of rat neonatal cardiac myocytes. *J Mol Cell Cardiol* 32:511-519.
3. Askari, B., Kanter, J.E., Sherrid, A.M., Golej, D.L., Bender, A.T., Liu, J., Hsueh, W.A., Beavo, J.A., Coleman, R.A., and Bornfeldt, K.E. 2007. Rosiglitazone inhibits acyl-CoA synthetase activity and fatty acid partitioning to diacylglycerol and triacylglycerol via a peroxisome proliferator-activated receptor-gamma-independent mechanism in human arterial smooth muscle cells and macrophages. *Diabetes* 56:1143-1152.
4. Jacotot, E., Ferri, K.F., El Hamel, C., Brenner, C., Druillennec, S., Hoebeke, J., Rustin, P., Metivier, D., Lenoir, C., Geuskens, M., et al. 2001. Control of mitochondrial membrane permeabilization by adenine nucleotide translocator interacting with HIV-1 viral protein rR and Bcl-2. *J Exp Med* 193:509-519.
5. Wu, Z., Puigserver, P., Andersson, U., Zhang, C., Adelmant, G., Mootha, V., Troy, A., Cinti, S., Lowell, B., Scarpulla, R.C., et al. 1999. Mechanisms controlling mitochondrial biogenesis and respiration through the thermogenic coactivator PGC-1. *Cell* 98:115-124.

6. Walther, T., Novo, M., Rossger, K., Letisse, F., Loret, M.O., Portais, J.C., and Francois, J.M. 2010. Control of ATP homeostasis during the respiro-fermentative transition in yeast. *Mol Syst Biol* 6:344.
7. Wu, L., Mashego, M.R., van Dam, J.C., Proell, A.M., Vinke, J.L., Ras, C., van Winden, W.A., van Gulik, W.M., and Heijnen, J.J. 2005. Quantitative analysis of the microbial metabolome by isotope dilution mass spectrometry using uniformly 13C-labeled cell extracts as internal standards. *Anal Biochem* 336:164-171.
8. Kiefer, P., Nicolas, C., Letisse, F., and Portais, J.C. 2007. Determination of carbon labeling distribution of intracellular metabolites from single fragment ions by ion chromatography tandem mass spectrometry. *Anal Biochem* 360:182-188.
9. Bligh, E.G., and Dyer, W.J. 1959. A rapid method of total lipid extraction and purification. *Can J Biochem Physiol* 37:911-917.
10. Lillington, J.M., Trafford, D.J., and Makin, H.L. 1981. A rapid and simple method for the esterification of fatty acids and steroid carboxylic acids prior to gas-liquid chromatography. *Clin Chim Acta* 111:91-98.
11. Harmancey, R., Wilson, C.R., Wright, N.R., and Taegtmeyer, H. 2010. Western diet changes cardiac acyl-CoA composition in obese rats: a potential role for hepatic lipogenesis. *J Lipid Res* 51:1380-1393.
12. Lamant, M., Smih, F., Harmancey, R., Philip-Couderc, P., Pathak, A., Roncalli, J., Galinier, M., Collet, X., Massabuau, P., Senard, J.M., et al. 2006. ApoO, a novel apolipoprotein, is an original glycoprotein up-regulated by diabetes in human heart. *J Biol Chem* 281:36289-36302.